

## NASA Advanced Propeller Research

John F. Groeneweg and Lawrence J. Bober  
*Lewis Research Center*  
*Cleveland, Ohio*

Prepared for  
Advanced Propellers and Their Installation on Aircraft  
sponsored by the Royal Aeronautical Society  
Cranfield Institute of Technology, England, September 26-27, 1988



## NASA ADVANCED PROPELLER RESEARCH

John F. Groeneweg and Lawrence J. Bober  
National Aeronautics and Space Administration  
Lewis Research Center  
Cleveland, Ohio 44135

### SUMMARY

E-4393

Acoustic and aerodynamic research at NASA Lewis Research Center on advanced propellers is reviewed including analytical and experimental results on both single and counterrotation. Computational tools used to calculate the detailed flow and acoustic fields are described along with wind tunnel tests to obtain data for code verification. Results from two kinds of experiments are reviewed: (1) performance and near field noise at cruise conditions as measured in the NASA Lewis 8- by 6-Foot Wind Tunnel and (2) far field noise and performance for takeoff/approach conditions as measured in the NASA Lewis 9- by 15-Foot Anechoic Wind Tunnel. Detailed measurements of steady blade surface pressures are described along with vortex flow phenomena at off-design conditions. Near field noise at cruise is shown to level out or decrease as tip relative Mach number is increased beyond 1.15. Counterrotation interaction noise is shown to be a dominant source at takeoff but a secondary source at cruise. Effects of unequal rotor diameters and rotor-to-rotor spacing on interaction noise are also illustrated. Comparisons of wind tunnel acoustic measurements to flight results are made. Finally, some future directions in advanced propeller research such as swirl recovery vanes, higher sweep, forward sweep, and ducted propellers are discussed.

### INTRODUCTION

For more than a decade NASA has pursued advanced propeller research. The work began in the mid-1970's as one component of the Aircraft Energy Efficiency Program managed by NASA Lewis. Driven by the high cost of fuel following the Middle East oil embargo, the goal of the work was to extend the high propulsive efficiency realizable by propellers to the Mach number 0.6 to 0.8 range of interest for commercial transport aircraft. Systems studies indicated that fuel savings of 15 to 30 percent were possible compared to current turbofans and up to 50 percent savings in fuel were achievable when advanced propellers were combined with advanced engine core technology.

NASA Lewis and Hamilton Standard began designing and testing model "prop-fans" around 1975. Based on encouraging results of wind tunnel tests of models having 8 to 10 thin, highly-loaded, swept blades, NASA began the Advanced Turboprop (ATP) Project in 1978. The goals of the project were to verify: (1) propeller performance and fuel savings; (2) structural integrity of the radically different blade designs; and (3) passenger and community environmental acceptability (i.e., cabin noise and vibration comparable to modern turbofan powered aircraft and compliance with airport community noise regulations).

Details of the ATP project and the systems approach used are given in references 1 and 2. All three NASA Research Centers were involved (Lewis,

Langley, and Ames) along with some 40 contracts distributed over the U.S. aircraft industry and 15 university grants. The plan was to achieve technology readiness in the late 1980's including flight demonstrations. Figure 1 indicates that in all three major technology efforts, single rotation, gearless counterrotation and geared counterrotation, the progression of work moved from analytical and system studies to design code development and verification based on scale model wind tunnel tests. From that technology base, large scale systems were designed, built and tested first on the ground and finally in flight.

Since 1986, the three series of flight tests pictured in figure 2 have been completed and a fourth is scheduled for late 1988. The NASA/Lockheed-Georgia Propfan Test Assessment (PTA) used a large scale advanced propeller (LAP) built by Hamilton Standard and mounted on the Gulfstream II test bed aircraft (ref. 3). Structural integrity was verified and extensive acoustic data were acquired in the near and far fields and inside the aircraft. Both the NASA/General Electric (GE)/Boeing 727 test and the GE/McDonnell-Douglas MD-80 tests used the GE unducted fan (UDF) gearless counterrotation concept (ref. 4). The Pratt & Whitney/Allison design is a geared counterrotation propulsion system (the 578-DX) with Hamilton Standard propellers and is scheduled for tests on the MD-80 (ref. 5).

This brief description of the overall ATP Program and associated industry activities serves as background for a review of the current and on-going NASA propeller research effort which is the subject of this paper. The research approach, as indicated pictorially in the upper half of figure 3, is the same as that pursued in providing the enabling technology for the ATP Program. It consists of analytical studies and scale model wind tunnel testing leading to validation of the propeller designs and verification of aerodynamic, acoustic, and structural codes. This paper reviews propeller acoustic and aerodynamic research at NASA Lewis using illustrative single- and counterrotation results obtained as part of the base technology portion of the ATP Program (ref. 6). Planned work on advanced concepts such as single rotation with swirl recovery vanes and ducted props (ultra high bypass fans) shown in the lower portion of figure 3 will also be discussed. Structural research, while no less important than the aerodynamic and acoustic work, is beyond the scope of this review and is treated elsewhere (e.g., refs. 7 and 8).

## PROPELLER ANALYSIS

Because these advanced high speed propellers are geometrically different than conventional propellers and operate at significantly different conditions than conventional propellers, new analysis methods were necessary to predict their aerodynamic and acoustic characteristics.

### Aerodynamic Codes

The propeller aerodynamic analysis methods developed as part of the NASA Advanced Turboprop Project are summarized in table I. All the methods included in this table are three-dimensional. The applicability of the methods to single rotation (SR) or counterrotation (CR) is indicated.

The four methods at the top of the table are classified as steady flow methods since in them each blade experiences no change in flow conditions as it rotates. This means that the nacelle is axisymmetric, there is no circumferential variation in flow field properties ahead of the propeller, the propeller axis is at zero angle of attack relative to the flight or freestream flow direction, and all blades in a propeller are identical.

Two lifting line methods have been developed (refs. 9 and 10). Both of these methods represent each propeller blade by a single line of bound vorticity at the blade quarter-chord location and include effects of twist and sweep. The blade vortex wakes are represented by a finite number of helical vortex filaments at specified locations. Radially varying axial inflow velocities due to nacelle contouring are included. These two methods differ in the way induced effects are included in the determination of blade aerodynamic forces. One method uses induced velocities to determine an induced angle of attack which is used with two-dimensional airfoil data to determine the forces; the other uses the assumption of flow tangency at the three-quarter chord location to determine the local lift and two-dimensional airfoil data to determine the local drag. Although these methods require a relatively small amount of computer time for execution, their treatment of compressibility is approximate and the results give a limited amount of flow field information.

A transonic potential analysis for single rotation propellers (ref. 11) has been developed to more accurately account for compressibility effects encountered at the high subsonic cruise Mach numbers at which these propellers operate. This approach also requires that the blade vortex wake location be specified and the computer program uses a rigid helix representation of this wake. This approach yields detailed blade surface flow properties as well as detailed information in the flow field around the propeller. An important flow field feature which can be identified is the shock wave pattern caused by the blades as they move through the air. The shock waves can indicate a less than optimum design both aerodynamically as well as acoustically. At some operating conditions the assumption of a rigid helical wake can cause inaccurate results. Although transonic potential methods can be faster than Euler methods, continuing development of the transonic potential propeller analysis has been discontinued in favor of Euler methods.

Use of the Euler equations to predict propeller flow fields eliminates the need for wake modeling. Detailed propeller blade and flow field information is again predicted. Four different computer programs (refs. 12 to 15) differing in the numerical method employed to solve the compressible Euler equations are being used to predict high speed propeller flow fields. Shock wave location and strength are predicted as well as blade wake, leading edge vortex and tip vortex rollup.

The final method for predicting propeller steady aerodynamics involves the use of the Navier-Stokes equations. Although not yet operational, a computer program based on the analysis of reference 14 and including the viscous terms of the Navier-Stokes equations is nearly complete. This approach promises new insight into propeller flow fields especially in the areas of blade boundary layers and blade viscous wakes as well as improved accuracy for blade leading edge and tip vortex development.

The final two methods to be discussed are considered unsteady since the aerodynamic forces experienced by the blades vary with time. Both are based on the method of reference 15. These are not unsteady due to changes in blade shape as in the case of blade flutter, but due to changes in the flow field which is a forced response problem.

Solutions of unsteady problems have been demonstrated using the Euler equation method. The key to solving these complex problems is the use of a blocked grid approach. In this approach the grid is composed of several blocks, only one of which is in the computer main memory at a time. This allows much larger grid sizes than could be used if the entire grid were in memory at one time. It also allows, in the case of the counterrotation propeller, for the blocks associated with the front propeller blades to move relative to the blocks associated with the rear propeller.

The final method included is the unsteady, Navier-Stokes analysis. This is planned as an extension of the reference 15 method described above. This method promises new insight into the time varying viscous effects associated with advanced propeller aerodynamics.

Current emphasis in the area of propeller aerodynamic analysis methods is on the Euler methods. This approach gives detailed flow field results with a minimum of assumptions and with computer times which are not unreasonable.

#### Acoustic Codes

Current propeller noise models emphasize two source components: thickness noise defined by propeller geometry and loading noise determined by aerodynamic loading which may be steady or unsteady. Each of the aerodynamic methods listed in table I may be used as a source of propeller blade loading input to an acoustic calculation as indicated in table II. The steady flow regime applies only to single rotation propellers in uniform flow. A steady flow treatment of counterrotation neglects the important interaction noise source and accounts for only the phased contributions of two rotors with steady loading. The unsteady flow regime exists in counterrotation and most practical installations of propellers on aircraft. Angle of attack, nonuniform inflow, and wake/vortex interactions with propeller blades are sources of unsteady loading.

The acoustic models are, with few exceptions, linear and of two varieties: time domain (ref. 16) or frequency domain (ref. 17). In the steady regime, both lifting line (A, table II) and Euler (C1) solutions have been used as input to the time domain model (refs. 18 to 20). A three-dimensional, linear lifting surface theory (B) yielding a unified aerodynamic and acoustic solution has been developed under a NASA Lewis contract with Hamilton Standard. Blade wakes (inviscid) are predicted, viscous wakes are semi-empirically modelled, and recently, a model for leading edge and tip vortices has been added. The code, which has subroutines to calculate wing shielding and fuselage boundary layer refraction, is being evaluated at Hamilton Standard and NASA Lewis. An effort to account for nonlinear near field propagation using a direct Euler code solution coupled to linear far field propagation (C3) is under development under a NASA Lewis grant at Texas A&M University (ref. 21). Navier-Stokes input to time domain acoustics (D) must await the development of the flow solver.

In the unsteady regime, the aerodynamic analyses are less developed and the approaches more varied. The three approaches labeled (E1 to E3) are efforts being largely developed under NASA Lewis contracts with General Electric. The uninstalled counterrotation code uses a mix of aerodynamic methods: section lift and drag determined by separate means are input as a function of radius for each rotor along with a choice of chordwise loading distribution. A semi-empirical wake-vortex model gives gust input to the downstream blade row whose unsteady loading is given by a linear lift response function. Unequal blade numbers or rotor speeds are handled. Installed single- and counterrotation codes (E2 and E3) use an actuator disk and either quasi-steady or linear lift response to calculate unsteady loading contributions to the noise for angle of attack or nonuniform inflow situations. The unsteady linear lifting surface theory (F) for unified aeroacoustic calculations has been completed at Hamilton Standard and work on the counterrotation extension is underway. The recent development of unsteady Euler solutions (G) for single- and counterrotation, described previously, offers the possibility of using the calculated instantaneous blade surface pressures as input to the linear time domain acoustics code. Work on the single rotation case at angle of attack is underway at NASA Lewis. Unsteady Navier-Stokes input to acoustics (H) is a long term plan.

From the indications of status in table II, it is clear that much work remains to be done in the unsteady regime with respect to counterrotation and installed configurations.

#### SINGLE-ROTATION TECHNOLOGY

Table III lists the design parameters for a series of single rotation propellers that have been tested at NASA Lewis. Several of the model blades are shown in figure 4. The most recent in the series of single rotation designs is SR-7A which is an aeroelastically scaled model of the 9-Foot diameter SR-7L Large Scale Advanced Propeller (LAP) which was used in the PTA Flight Program using the Gulfstream II testbed aircraft (ref. 3).

#### Cruise Performance and Noise

Extensive wind tunnel test programs were conducted on SR-7A. Figure 5 shows the SR-7A installed in the NASA Lewis 8- by 6-Foot Wind Tunnel, where its aerodynamic, acoustic, and aeroelastic performance were measured at cruise conditions. The tunnel walls have about 6 percent porosity to minimize wall interactions with the model at transonic speeds. The laser beams are part of a system used to measure mean blade deflection during propeller operation, i.e., the so-called "hot" blade shape.

Net efficiency of the SR-7A propeller model is shown in figure 6 along with results from five earlier models (ref. 22). Measured net efficiencies are shown as a function of freestream Mach number with each propeller's design loading parameter,  $C_p/J^3$ , kept constant with Mach number. At Mach 0.80, the design point for SR-7A, its efficiency lies on the upper bound of measured efficiencies with a value of 79.3 percent. The SR-2 propeller has the lowest performance because it is the only one of these models which has no blade sweep.

A comparison of predicted and measured power coefficients for the SR-3 propeller at a freestream Mach number of 0.80 is shown in figure 7. The predicted results were obtained using a three-dimensional Euler analysis (ref. 12) and the experimental results were obtained during model tests in the NASA Lewis 8- by 6-Foot Wind Tunnel (ref. 23). To obtain the predicted results the blades were assumed to deflect as propeller rotational speed increased. The deflections were determined at the design point ( $J = 3.06$ ,  $C_p = 1.7$ ) and were scaled to determine deflections at other operating conditions. The agreement between predicted and measured power coefficient is quite good even at the high power conditions where the analysis slightly overpredicts the power absorbed by the propeller.

The technique used to measure near field noise at cruise in the NASA Lewis 8- by 6-Foot Wind Tunnel is shown in figure 8 (ref. 24). A row of twelve transducers were installed flush with the surface and on the centerline of a plate which was mounted from the tunnel ceiling. The centerline of the transducer row was parallel to the propeller centerline at a distance 0.3 propeller diameters from the propeller tip. Use of the plate was preferable to making measurements at the porous wind tunnel wall for two reasons. The plate provided a well defined "hard" wall condition to produce pressure doubling and it reduced effects of boundary layer refraction at angles forward of the propeller by establishing a thinner boundary layer over the forward transducers. This technique has been shown to be valid for measuring tone levels around the peak by comparisons with model flight data (ref. 25).

The peak fundamental tone levels for SR-7A are plotted in figure 9 as a function of helical tip Mach number (ref. 24). Advance ratio is constant at 3.06 and the near field measurements were made on a sideline parallel with the propeller axis at 0.3 propeller diameter from the propeller tip by the method just described. Data for three loading levels are shown as indicated by the blade setting angles bracketing the design value. The striking feature of the tone variation with helical tip Mach number is the behavior in the supersonic range beyond 1.1. The peak fundamental tone levels no longer increase and may peak, level off, or decrease depending on loading. An examination of the performance data shows that efficiency remains nearly constant along each of the noise curves. This result indicates that higher cruise and propeller speeds do not necessarily mean increased cabin noise problems. To date, linear aeroacoustic codes do not predict these tone characteristics at helical tip Mach numbers above 1.15.

Data on SR-7A from the 8- by 6-Foot wind tunnel has been scaled-up to compare with some early fundamental tone level data measured on the fuselage of the Gulfstream II in the PTA flight tests with SR-7L. Figure 10 shows favorable agreement between the model and full scale blade passing tone directivities, particularly in the vicinity of the peaks. The dashed curve in the figure is an early Hamilton Standard prediction (ref. 26). As more PTA flight data become available, the scaling comparison will be made over a range of conditions.

#### Takeoff Noise and Performance

The SR-7A propeller model was also tested in the NASA Lewis 9- by 15-Foot Anechoic Wind Tunnel to measure far field noise and performance at typical takeoff and approach conditions (Mach 0.2). Figure 11 shows the model

installed on a swept wing used to determine installation effects. The entire propeller-wing assembly may be rotated to angle of attack in the horizontal plane. The continuously traversing microphones (at right) measure far field noise corresponding to levels measured below an aircraft during flyover. Three fixed microphone arrays are shown on the left wall, ceiling, and floor. Each array is staggered with respect to the tunnel flow to avoid wake interference on downstream microphones. The walls are acoustically treated with a double layer bulk absorber design (ref. 27) to provide anechoic conditions down to a frequency of 250 Hz, well below the fundamental frequency (1000 Hz at design speed) for the propeller model.

The effect of angle of attack on the flyover noise of SR-7A without the wing is shown in figure 12 (ref. 28). Fundamental tone directivities are shown for four angles of attack ranging from 0 to 15°. The peak levels, approximately in the plane of rotation, increased by about 10 dB. A typical maximum takeoff angle of the propeller centerline with respect to the aircraft flight path is about 8°; thus takeoff noise would be increased of the order of 5 dB due to unsteady loading at that angle of attack.

Fully unsteady, three-dimensional Euler code solutions have recently been obtained for advanced propeller geometries (ref. 15). Results from the unsteady Euler code solution for the SR-3 propeller with its axis at 4° to the mean 0.8 Mach number flow are shown in figure 13. As the propeller rotates, downward moving blades (on the right in the figure) experience the highest incidence, upward blades (on the left) the lowest, and top and bottom are near the mean. Pressure contours for regions where the absolute flow velocities are supersonic are plotted in alternate blade passages. Large regions of supersonic flow are shown for the high incidence, high loading positions with much smaller supersonic regions corresponding to lower incidences and loadings. While this initial calculation was for cruise conditions, the general description of the mechanism leading to unsteady loading is similar at takeoff. Codes such as this have the potential to provide instantaneous blade surface pressures to be used as the starting point for acoustic calculations.

In addition to simple angle of attack of the propeller axis with the mean flow, the low speed acoustics of SR-7A were investigated for a tractor installation on a straight wing. Angle of attack of the propeller axis and wing assembly were varied along with the droop angle of the propeller axis with respect to the wing chord. Analogous variations of nacelle tilt have been investigated in the PTA program (ref. 3). Results of the model tests are shown in figure 14 where maximum tone noise at the fundamental and second harmonic are plotted as a function of angle of attack for various droop angles. The addition of the wing increases tone levels with respect to the no-wing baseline, but the angle of attack of the propeller axis appears to be the dominant parameter controlling the maximum tone levels with droop angle having a much weaker influence at these low speed ( $M = 0.2$ ) conditions.

A three-dimensional Euler code was used to define the blade pressures for input to a time domain acoustic calculation for SR-7A over a range of loadings investigated in the NASA Lewis 9- by 15-Foot Anechoic Wind Tunnel (ref. 29). Figure 15 indicates that the predicted power coefficients were in reasonable agreement with the measured values for three blade angles (loadings) over a range of advance ratios.

The computed tone levels at constant advance ratio,  $J = 0.886$ , are shown for increasing blade pitch angles in figure 16. While fundamental tone agreement between data and predictions is good at the lowest loading ( $\beta = 32.0^\circ$ ), there is an increasing tendency to underpredict as loading is increased.

### Blade Pressures/Off-Design Operation

A detailed knowledge of propeller blade surface pressures is important for aerodynamic code validation and as input to acoustic calculations. A two-blade version of the eight-blade large-scale advanced propeller (LAP) was tested in the ONERA S1 wind tunnel (see fig. 17) to obtain steady and unsteady blade pressures over a wide range of operating conditions (ref. 30). Only two blades were used because of the limited total power available to drive the propeller. In this way the propeller could be operated at a reasonable power per blade. The large size of this propeller (9 ft diameter) provided a unique opportunity to measure surface pressures in detail. Previously, only a limited number of unsteady measurements were available from experiments on the 2-ft-diameter models (ref. 31).

Sample results of the steady blade pressure distributions measured are shown in figure 18 (ref. 6) at several spanwise locations on the LAP at a low-speed, high-power condition. The pressure distributions at the two locations nearest the tip lack the high suction peaks of the inboard locations. The spanwise variation of chordwise loading at this off-design condition is associated with the presence of leading edge and tip vortices at the outboard locations. Measurements were obtained at 12 additional operating conditions, providing valuable data for code verification.

When a propeller is operating appreciably off-design such as at takeoff, a leading edge vortex which merges with the tip vortex is expected to form. The phenomenon is similar to the vortex structure on a delta wing aircraft at high angle of attack. If the associated loading distribution is not accounted for in analytical models, errors in aerodynamic performance and/or the tone noise level predictions will result. Failure to adequately define such a complex propeller loading distribution is the suspected cause of the underprediction of the tone noise at high loading as shown in figure 16.

In addition to the blade pressure data, flow visualization of propeller blade surface flows at off-design conditions has indicated the presence of leading edge and tip vortices (refs. 22 and 32). Fluorescent oil flow patterns on the pressure side of the SR-3 blade at the Mach 0.8, windmill condition are shown in figure 19. Streaks in the oil at the blade surface are influenced by two main factors. Centrifugal forces cause radial flow in the oil film. Shear flow forces at the surface act mainly along streamlines. Over much of the blade the streaks are at an angle determined by these two forces. However, near the leading edge on the outboard portion of the blade and at the tip, the lines are primarily radial. This indicates a different flow regime, interpreted as the existence of a leading edge vortex merging with a tip vortex.

This flow phenomena has recently been predicted computationally. An Euler code developed at NASA Lewis (ref. 14) was run at United Technologies Research Center (UTRC) with an order of magnitude increase in grid points to

about 200 000. When particle paths were traced they revealed the leading edge vortex which merges with the tip vortex flow as shown in figure 20. The operating condition at Mach 0.2 and advance ratio of 1.0 is typical of a takeoff situation which involves high incidence angles. Apparently, numerical "viscosity" is sufficient to trigger vortex formation and produce at least a qualitative description of this flow phenomenon. It remains to be investigated whether the inviscid Euler code solution accurately captures the main features of the vortex flow and, therefore, is useful for acoustic predictions at conditions such as takeoff.

## COUNTERROTATION TECHNOLOGY

Table IV lists design parameters for two counterrotation propellers. The F7/A7 is a scale model of the propeller used on the GE UDF demonstrator engine (ref. 4). It is one of a series of models which were tested at NASA Lewis. The CRP-X1 model simulates a counterrotation tractor propeller. It was designed and built by Hamilton Standard under contract to NASA Lewis and was tested in aerodynamic and acoustic wind tunnels at United Technologies Research Center (refs. 33 and 34). This propeller represented the first step in a Hamilton Standard series of counterrotation blade developments for the geared Pratt & Whitney/Allison 578DX demonstrator.

### Cruise Performance and Noise

In figure 21 the NASA Lewis counterrotation pusher propeller test rig is shown installed in the 8- by 6-Foot Wind Tunnel. The propeller shown is the F7/A7 configuration described in table IV. The rig is strut mounted and is powered by two 675 hp air turbines using 450-psi drive air. Performance, flow field, and acoustic measurements were made.

Examples of the blade configurations tested are shown in figure 22 and included designs for Mach 0.72 cruise (top row) and Mach 0.8 cruise (bottom row). The designs differed in tip sweep, planform shape, airfoil camber, and a significantly shortened aft rotor (A3). The planform shapes for most forward and aft rotor pairs were very similar. The aft rotor planform for A21 is included since it differs so much from the front rotor F21. The F1/A1 configuration is very similar to F7/A7 but with reduced camber, which is expected to improve cruise efficiency. F1/A3 was run to determine the aerodynamic and acoustic effects of a short aft rotor. These blades were designed and built by the General Electric Company, several under contract to NASA Lewis.

To ensure the accuracy of the measured propeller performance parameters, a test program was undertaken in the NASA Lewis Research Center 8-by 6-Foot Wind Tunnel to check the wind tunnel calibration and to determine the interference effects between the model and the wind tunnel walls (ref. 35). Instrumentation used in the test included pitot-static rakes as well as a static pressure rail located near the test section wall. Both of these could be moved to different locations and could be used with and without the counterrotation model installed. Empty tunnel measurements indicated the existing tunnel calibration needed no modification. The measured radial distribution of velocity in the plane of the propeller without the propeller blades present was compared to an axisymmetric potential flow prediction of the flow at the same location as

indicated in figure 23. Since the measured velocity ratio did not agree with the predicted velocity ratio, the freestream velocity for the experimental results was adjusted until the two curves matched. This resulted in a new freestream velocity which accounted for the interference effects of the wind tunnel walls. The Mach number correction corresponding to this velocity difference is summarized in figure 24 which shows that the correction increases in magnitude with increasing Mach number but amounts to only 0.008 at Mach 0.80. This change in Mach number also effects the values of advance ratio and efficiency such that at a Mach 0.80 cruise condition the reduction in Mach number causes an efficiency reduction of 0.46 percent for the F7/A7 configuration at the same power coefficient and advance ratio. Additional results indicated that for this porous wall wind tunnel no correction to tunnel Mach number due to propeller thrust was required.

Net efficiencies for F7/A7 are shown in figure 25 as a function of Mach number for three loadings: design, 80 and 120 percent of design (ref. 6). Tip speed was held constant at the design value of 780 ft/sec. At the design Mach number of 0.72, efficiency depends quite strongly on loading: increased loading decreases efficiency. At Mach numbers significantly higher than design, compressibility losses dominate and efficiencies fall off nearly independent of loading.

A counterrotation Euler code developed at NASA Lewis (ref. 14) has been used to obtain numerical predictions of the flow about the F7/A7 version of the UDF. The solution is obtained by iterating between the front and rear blade rows. The coupling between rows is done in a circumferentially-averaged sense, so that each blade row sees a steady flow including the effect of the other propeller. Figure 26 shows the pressure distribution on the nacelle and blade surfaces as well as on a plane perpendicular to the axis of rotation at the aft end of the nacelle. The flow field pressures at the aft end of the nacelle were taken from the flow field of the rear row and, in the original color picture, showed near-field acoustic pressure perturbations spiraling out into the flow. The calculations were done at Cray Research, and the flow field was displayed using the code MOVIE-BYU.

Counterrotation fundamental tone levels at cruise conditions are shown in figure 27 (ref. 36). Fundamental tone directivities for F7/A7, the proof-of-concept UDF configuration, are compared for: model data from the NASA Lewis 8- by 6-Foot Wind Tunnel scaled to full-scale cruise conditions, full-scale flight data obtained by the formation flight of the instrumented NASA Lewis Learjet with the UDF engine on the 727, and predicted levels from a frequency domain model developed by General Electric. There is good agreement between the model wind tunnel measurements and full-scale flight data. Predicted levels agree quite well with the data except at the forward angles.

The counterrotation spectrum contains rotor-alone tones and their harmonics plus interaction tones at all integer sums of the rotor fundamentals. Cruise noise measurements in the 8- by 6-Foot Wind Tunnel indicate that rotor-alone tones dominate the spectrum over a broad range of angles around the plane of rotation. This point is illustrated in figure 28 which shows the tone directivities measured on the F1/A1 configuration run with 9 forward and 8 aft blades (9/8) which distinctly separated all tones in the spectrum (ref. 37). The directivities of the second harmonics, the first interaction tone and the sum of the three are shown. The interaction tone is more than 10 dB down from

the second harmonics around the plane of rotation. Rotor alone fundamentals (not shown) are of the order of 10 dB higher than the rotor alone second harmonics. In short, interaction noise at cruise is only a contributor near the propeller axis.

### Takeoff Performance and Noise

Noise and performance measurements were also made on several counterrotation models at takeoff/approach conditions. In figure 29 the F7/A7 model in the 8/8 configuration is shown in the 9- by 15-Foot Anechoic Wind Tunnel where extensive community noise tests were conducted (refs. 38 and 39). Unequal blade numbers, differential diameter, rotor-to-rotor spacing, angle of attack, and effects of an upstream support pylon were investigated. In addition to the traversing flyover microphone, a polar microphone probe attached to the model could traverse axially and circumferentially to map the asymmetric sound field generated by the model at angle of attack.

Propeller efficiencies at takeoff are shown in figure 30 for several F7/A7 configurations. More detailed performance results are reported in reference 40. The data presented in figure 30 are measured net efficiencies for three configurations at a freestream Mach number of 0.20 for a range of power loading parameter values. The two F7/A7, 8/8 curves indicate the effect of rotational speed since, at any value of  $C_p/J^3$ , the two sets of blade angles require different rotational speeds. Comparing the F7/A7, 8/8 and the F7/A7, 11/9 curves gives an indication of the effect of changing the number of blades. Finally, comparing the F7/A7, 11/9 and F7/A3, 11/9 curves gives the effect of reducing the aft propeller diameter. This data indicates that low speed performance is not sensitive to significant changes in propeller geometry; the largest efficiency difference between all the geometries shown is less than 3 percent.

Also investigated during the low speed wind tunnel test was propeller reverse thrust performance of the F7/A7 propeller over the range of Mach numbers from 0.0 to 0.2. A summary of these results is shown in figure 31 (ref. 40). Here reverse thrust is normalized by the forward thrust generated at takeoff conditions (Mach 0.20). Data are shown for two sets of blade angles at two rotational speeds. Very large amounts of reverse thrust, up to 60 percent of takeoff thrust at Mach 0.20, can be generated. This is significantly more than can be generated by a turbofan engine. Even at the flat pitch blade angles which require only a small amount of power, over 30 percent of the takeoff thrust can be generated in reverse thrust at Mach 0.20.

Examples of counterrotation propeller noise at the takeoff conditions are shown in figure 32 (see ref. 38). Measured and predicted directivities of the front rotor fundamental and the first interaction tone for F7/A7 at Mach 0.2 are compared. The predictions are from a frequency domain theory acquired under a contract with General Electric. Note the high levels of interaction tone noise at both forward and aft angles, in contrast to the forward rotor-alone fundamental which peaks in the plane of rotation. In contrast to the cruise condition as discussed in connection with figure 28, the levels of the first interaction tone are comparable to the peak of the rotor fundamental. Agreement between theory and data is very good for the front rotor fundamental. The predicted shape of the first interaction tone agrees well with the

data, but the levels are underpredicted at the extremes in angle indicating more code development work is required to predict the interaction noise sources.

Angle of attack experiments were conducted for the F7/A7 propeller over range of angles from  $-16^\circ$  (diving) to  $+16^\circ$  (climbing) (ref. 38). While operational angles would be considerably smaller in passenger aircraft, it was of general interest to investigate a wide range as was done for SR-7A. Figure 33 compares rotor fundamental tone with interaction tone variations measured in the aft propeller plane simulating a position below an aircraft. Both rotor-alone fundamental tone sound pressure levels change almost linearly with angle of attack. The interaction tones show only modest variations as would be consistent with a situation where each rotor behaved as a single rotation propeller at angle of attack and disturbances from the forward rotor which interact with the downstream rotor were only moderately altered by operation at angle of attack.

An example of circumferential tone directivity for F7/A7 at  $16^\circ$  angle of attack measured in the plane of A7 is shown in figure 34 (ref. 38). The full  $360^\circ$  directivities were obtained by combining corresponding positive and negative angle of attack data taken over a  $240^\circ$  traverse. The two rotor fundamental tone directivities become strongly asymmetric with respect to the dashed circle representing the zero angle of attack directivity of the forward rotor tone. Levels increase at  $180^\circ$  (below a climbing aircraft) and decrease at  $0^\circ$  (above the aircraft) as for single rotation. The distortion in the patterns depends on direction of rotation and whether the rotor is fore or aft. Note that the interaction tone is also asymmetric. Modeling this complex behavior for counterrotation propellers at angle of attack continues to be the subject of ongoing work.

The effect of reduced aft diameter and rotor-to-rotor spacing on counterrotation interaction noise is shown in figure 35 (ref. 39). Tone data from F7/A7 and F7/A3, both in 11/9 configurations, is plotted versus axial spacing between blade pitch axes. The reduced diameter, wide chord blade, A3, is shown in figure 22. If rotor-to-rotor interaction noise is strongly influenced by tip flow disturbances from the forward rotor such as vortices in addition to the spanwise viscous wakes, a shortened aft rotor could avoid the vortex interaction. As spacing is increased interaction tones would be expected to fall off at a faster rate because viscous wake decay with downstream distance is more rapid than vortex decay. For the data in figure 35, F7/A7 and F7/A3 were absorbing the same power at the same rotational speed and produced equal thrust by setting A3 at a higher pitch than A7. As expected, figure 35(a) shows that fundamental rotor-alone tones are not influenced by spacing. The first two interaction tones, shown in figure 35(b), do decrease more rapidly with spacing and reach lower levels for F7/A3 compared F7/A7. However, at the closest spacing F7/A3 has higher interaction tone levels possibly associated with potential field interaction of F7 with the highly loaded A3.

At present, analytical descriptions of the unsteady flow field interactions between counterrotating propellers rely to varying degrees on semi-empirical modeling and/or simplifying assumptions. An important computational step has been taken by extending to counterrotation the unsteady, three-dimensional Euler solution algorithms used for the single-rotation propeller at angle of attack (fig. 13). A fully unsteady, three-dimensional solution for the flow

field of the F7/A7, 8/8 counterrotation propeller was obtained. A sample of the results in the form of pressure contours in a plane just downstream of both blade rows is shown in figure 36 (ref. 15). These contours, which are for a particular instant in time, show a low pressure island structure indicative of the tip vortices shed by the blades. Current solution methods handle equal blade numbers in each row and are being extended to treat the general case of unequal blade numbers.

## ADVANCED CONCEPTS

The ongoing propeller research program at NASA will continue to improve and verify aerodynamic and acoustic codes using the extensive model and full scale data base acquired during the ATP Program. In addition, the research is turning to advanced concepts for second generation applications now that the first generation of advanced single and counterrotation propellers has been demonstrated.

A swirl recovery vane experiment will be conducted to determine if a set of nonrotating vanes provide a means of realizing some of the swirl recovery benefits of counterrotation with a mechanically simpler and, perhaps, quieter propeller configuration. A set of vanes will be added behind a single-rotation propfan model (SR-3) as shown in figure 37. The existing 1000 hp, single-rotation propeller test rig will be modified to accept eight swept vanes mounted on an independent thrust balance. Propeller efficiencies and noise will be measured at cruise Mach numbers up to 0.85 and at takeoff/approach conditions. Vane pitch angles and propfan-to-vane axial spacings will be varied. Design calculations indicate that as much as two-thirds of the 8 to 10 percent efficiency increment available from counterrotation can be realized with the stationary swirl recovery vanes. Interaction noise is also predicted to be considerably lower than for counterrotation propellers.

Higher sweep and forward sweep are two additional concepts being studied. If tip sweep can be pushed to the 50 to 60° range while retaining aeroelastic stability, significant tone noise reduction (8 dB relative to SR-3) is predicted. A previously unstable propeller (SR-5) is being redesigned using composite materials and design techniques developed in the ATP Program. A combined forward/aft swept counterrotation propeller is under study as a potentially low interaction noise configuration. Wider tip spacing offers the possibility of lower takeoff noise and forward sweep on the forward rotor may improve the aerodynamics.

Finally, another advanced concept which NASA is investigating is the ducted propeller (ultra high bypass fan). For long range aircraft with wing-mounted engines, ducted propellers have installation advantages in terms of limiting the diameter required for a given thrust and thus, satisfying ground clearance requirements. Technical issues associated with these configurations which require research are noted for high-speed cruise in the upper half of figure 38 and for low-speed takeoff or approach in the lower half. At cruise, the drag of the large-diameter thin cowl must be minimized while achieving acceptable near-field sound levels. A synthesis of propeller and fan aerodynamic design methods is required to arrive at an optimum combination of sweep and of axial and tip Mach numbers. At low speed conditions, far-field

community noise, cowl-lip separation at high angles of attack with the associated blade stresses, and reverse thrust operation must each be addressed.

#### CONCLUDING REMARKS

This paper has given an overview of advanced propeller research at NASA Lewis by focusing on the technology base part of the overall ATP Program. Specifically, examples of acoustic and aerodynamic, analytical and experimental results were given for both single- and counterrotation. A large data base now exists for both scale models and full scale hardware. Initial comparisons of scale model wind tunnel acoustic data with full scale flight data are encouraging. A variety of three-dimensional computational codes for aerodynamic and acoustic predictions are available. Additional capabilities such as unsteady three-dimensional Euler, steady Navier-Stokes, and installed counterrotation acoustic codes are under development. On-going propeller research at NASA Lewis will both consolidate and verify the computational capabilities and move on to advanced concepts for second generation advanced propfan applications.

#### REFERENCES

1. Whitlow, J.B., Jr.; and Sievers, G.K.: Fuel Savings Potential of the NASA Advanced Turboprop Program. NASA TM-83736, 1984.
2. Whitlow, J.B., Jr.; and Sievers, G.K.: NASA Advanced Turboprop Research and Concept Validation Program. NASA TM-100891, 1988.
3. Poland, D.T.; Bartel, H.W.; and Brown, R.C.: PTA Flight Test Overview. AIAA Paper 88-2803, July 1988.
4. Reid, C.R.: Overview of Flight Testing of GE Aircraft Engines' UDF Engine. AIAA Paper 88-3082, July 1988.
5. Chapman, D.C.; Godston, J.; Smith, D.E.; and Bushnell, P.: Flight Test of 578DX Geared Prop-Fan Propulsion System. AIAA Paper 88-2804, July 1988.
6. Groeneweg, J.F.; and Bober, L.J.: Advanced Propeller Research. Aeropropulsion '87, Session 5, Subsonic Propulsion Technology, NASA CP-10003-SESS-5, 1987, pp. 5-123 to 5-152.
7. Ernst, M.A.; and Kiraly, L.J.: Determining Structural Performance. Aeropropulsion '87, Session 2, Aeropropulsion Structures Research, NASA CP-10003-SESS-2, 1987, pp. 2-11 to 2-24.
8. Kaza, K.R.V.; Mehmed, O.; Narayanan, G.V.; and Murthy, D.V.: Analytic Flutter Investigation of a Composite Propfan Model. AIAA Paper 87-0738, Apr. 1987. (NASA TM-88944).

9. Egolf, T.A.; Anderson, O.L.; Edwards, D.E.; and Landgrebe, A.J.: An Analysis for High Speed Propeller-Nacelle Aerodynamic Performance Prediction: Volume 1, Theory and Initial Application; Volume 2, User's Manual for the Computer Program. (R79-912949-19-VOL-1,-2, United Technologies Research Center; NASA Contract NAS3-20961) NASA CR-169450/NASA CR-169451, 1979.
10. Lesieutre, D.J.; and Sullivan, J.P.: The Analysis of Counter-Rotating Propeller Systems. SAE Paper 850869, Apr. 1985.
11. Jou, W.H.: Finite Volume Calculation of Three-Dimensional Potential Flow Around a Propeller. AIAA Paper 82-0957, June 1982.
12. Yamamoto, O.; Barton, J.M., and Bober, L.J.: Improved Euler Analysis of Advanced Turboprop Flows. AIAA Paper 86-1521, June 1986.
13. Denton, J.D.: Time Marching Methods for Turbomachinery Flow Calculations. Numerical Methods in Fluid Dynamics, B. Hunt, ed., Academic Press, New York, 1980, pp. 473-493.
14. Celestina, M.L.; Mulac, R.A., and Adamczyk, J.J.: A Numerical Simulation of the Inviscid Flow Through A Counter-Rotating Propeller. NASA TM-87200, June 1986.
15. Whitfield, D.L.; Swafford, T.W.; Janus, J.M.; Mulac, R.A.; and Belk, D.M.: Three-Dimensional Unsteady Euler Solutions for Propfans and Counter-Rotating Propfans in Transonic Flow. AIAA Paper 87-1197, June 1987.
16. Farassat, F.: Prediction of Advanced Propeller Noise in the Time Domain. AIAA J., vol. 24, no. 4, Apr. 1986, pp. 578-584.
17. Hanson, D.B.: Compressible Helicoidal Surface Theory for Propeller Aerodynamics and Noise. AIAA J., vol. 21, no. 6, June 1983, pp. 881-889.
18. Nystrom, P.A.; and Farassat, F.: A Numerical Technique for Calculation of the Noise of High-Speed Propellers with Advanced Blade Geometry. NASA TP-1662, 1980.
19. Clark, B.J.; and Scott, J.: Coupled Aerodynamic and Acoustical Predictions for Turboprops. NASA TM-87094, 1986.
20. Nallasamy, M.; Clark, B.J.; and Groeneweg, J.F.: High-Speed Propeller Noise Predictions: Effects of Boundary Conditions Used in Blade Loading Calculations. J. Aircraft, vol. 25, no. 2, Feb. 1988, pp. 154-162.
21. Korkan, K.D.; von Lavante, E.; and Bober, L.J.: Numerical Evaluation of Propeller Noise Including Non-Linear Effects. AIAA J., vol. 24, no. 6, June 1986, pp. 1043-1045.
22. Stefko, G.L.; Rose, G.E.; and Podboy, G.G.: Wind Tunnel Performance Results of an Aeroelastically Scaled 2/9 Model of the PTA Flight Test Prop-Fan. AIAA Paper 87-1893, June 1987. (NASA TM-89917).
23. Rohrbach, C.; Metzger, F.B.; Black, D.M.; and Ladden, R.M.: Evaluation of Wind Tunnel Performance Testings of an Advanced 45° Swept Eight-Bladed Propeller at Mach Numbers from 0.45 to 0.85. NASA CR-3505, 1982.

24. Dittmar, J.H.; and Stang, D.B.: Cruise Noise of the 2/9 Scale Model of the Large-Scale Advanced Propfan (LAP) Propeller, SR-7A. AIAA Paper 87-2717, Oct. 1987.
25. Dittmar, J.H.: Further Comparison of Wind Tunnel and Airplane Acoustic Data for Advanced Design High Speed Propeller Models. NASA TM-86935, 1985.
26. Parzych, D.; Cohen, S.; and Shenkman, A.: Large-Scale Advanced Propfan (LAP) Performance, Acoustic, and Weight Estimation. NASA CR-174782, 1985.
27. Dahl, M.D.; and Rice, E.J.: Measured Acoustic Properties of Variable and Low Density Bulk Absorbers. NASA TM-87065, 1985.
28. Woodward, R.P.: Measured Noise of a Scale Model High Speed Propeller at Simulated Takeoff/Approach Conditions. AIAA Paper 87-0526, Jan. 1987. (NASA TM-88920).
29. Nallasamy, M.; Woodward, R.P.; and Groeneweg, J.F.: High-Speed Propeller Performance and Noise Predictions at Takeoff/Landing Conditions. AIAA Paper 88-0264, Jan. 1988. (NASA TM-100267).
30. Campbell, W.A.; Wainauski, H.S.; and Bushnell, P.R.: A Report on High Speed Wind Tunnel Testing of the Large Scale Advanced Prop-Fan. AIAA Paper 88-2802, July 1988.
31. Heidelberg, L.J.; and Woodward, R.P.: Advanced Turboprop Wing Installation Effects Measured by Unsteady Blade Pressure and Noise. AIAA Paper 87-2719, Oct. 1987. (NASA TM-100200).
32. Vaczy, C.M.; and McCormick, D.C.: A Study of the Leading Edge Vortex and Tip Vortex on Prop-Fan Blades. J. Turbomachinery, vol. 109, no. 3, July 1987, pp. 325-331.
33. Wainauski, H.S.; and Vaczy, C.M.: Aerodynamic Performance of a Counter Rotating Prop-Fan. AIAA Paper 86-1550, June 1986.
34. Magliozzi, B.: Noise Characteristics of a Model Counter-Rotating Prop-Fans. AIAA Paper 87-2656, Oct. 1987.
35. Stefko, G.L.; and Jeracki, R.J.: Porous Wind Tunnel Corrections for Counterrotation Propeller Testing. AIAA Paper 88-2055, May 1988. (NASA TM-100873).
36. Woodward, R.P.; Loeffler, I.J.; and Dittmar, J.H.: Cruise Noise of an Advanced Counterrotation Turboprop Measured From an Adjacent Aircraft. NOISE-CON 88, J. Stuart Bolton, ed., Purdue University, 1988, pp. 105-110.
37. Dittmar, J.H.; and Stang, D.B.: Noise Reduction for Model Counterrotation Propeller at Cruise by Reducing Aft-Propeller Diameter. NASA TM-88936, 1987.
38. Woodward, R.P.: Noise of a Model High Speed Counterrotation Propeller at Simulated Takeoff/Approach Conditions (F7/A7). AIAA Paper 87-2657, Oct. 1987. (NASA TM-100206).

39. Woodward, R.P.; and Gordon, E.B.: Noise of a Model Counterrotation Propeller with Reduced Aft Rotor Diameter at Simulated Takeoff/Approach Conditions (F7/A3). AIAA Paper 88-0263, Jan. 1988. (NASA TM-100254).
40. Hughes, C.E.; and Gazzaniga, J.A.: Summary of Low-Speed Wind Tunnel Results of Several High-Speed Counterrotation Propeller Configurations. AIAA Paper 88-3149, July 1988. (NASA TM-100945).

TABLE I. - PROPELLER AEODYNAMIC ANALYSIS METHODS

	Type	SR/CR	Status
Steady	Lifting line	Both	Operational
	Transonic potential	SR	Operational
	Euler	Both	Operational
	Navier-Stokes	Both	Under development
Unsteady	Euler	Both	Operational
	Navier-Stokes	Both	Planned

TABLE II. - PROPELLER ACOUSTIC ANALYSIS METHODS

(a) Steady regime

Aerodynamic input	Acoustic model		Single (SR) or counterrotation (CR)	Status <sup>a</sup>
	Type	Domain		
(A) Lifting line	Linear	Time	SR	0
(B) Lifting surface	↓	Frequency		UD
(C1) Euler		Time		
(C2) Euler		Frequency		
(C3) Euler	Nonlinear/Linear	Time	↓	P
(D) Navier-Stokes	Linear	Time		

(b) Unsteady regime

(E1) Hybrid aero/ linear lift response	Linear ↓	Frequency	CR	0
(E2) Actuator disk/ linear lift response		Frequency	SR <sup>b</sup>	0
(E3) Actuator disk/ linear lift response		Frequency	CR <sup>b</sup>	UD
(F) Lifting surface		Frequency	SR <sup>b</sup> CR <sup>b</sup>	0 UD
(G) Euler		Time	SR CR	UD P
(H) Navier-Stokes		Time	SR CR	P P

<sup>a</sup>Status: 0-Operational UD-Underdevelopment, P-Planned.

<sup>b</sup>Installed.

TABLE III. - SINGLE-ROTATION PROPELLER DESIGN PARAMETERS

Design	Number of blades	Sweep angle, deg	Power coefficient, $C_p$	Advance ratio, $J$	Loading parameter, $C_p/J^3$	Tip speed, ft/sec	Cruise loading shp/D <sup>2</sup>
SR-7A	8	41	1.45	3.06	0.0509	800	32.0
SR-6	10	40	2.03	3.50	.0474	700	30.0
<sup>a</sup> SR-6	10	40	2.03	3.50	.0474	700	30.0
SR-3	8	45	1.70	3.06	.0593	800	37.5
SR-1M	8	30	1.70	3.06	.0593	800	37.5
SR-2	8	0	1.70	3.06	.0593	800	37.5

<sup>a</sup>Estimated performance with alternate spinner 2.

TABLE IV. - ADVANCED COUNTERROTATION PROPELLER DESIGN

## PARAMETERS

Design	Number of blades	Radius ratio	Cruise Mach number	Cruise loading, shp/D <sup>2</sup>	Tip speed, ft/sec
F7/A7	8/8	0.425	0.72	55.5	780
CRP-X1	5/5	.240 .275	.72	37.2	750

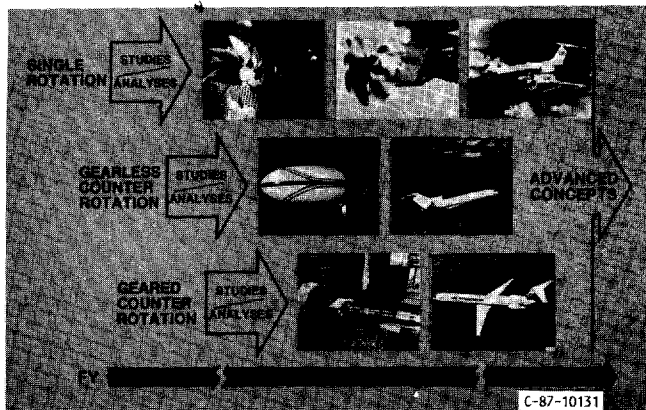
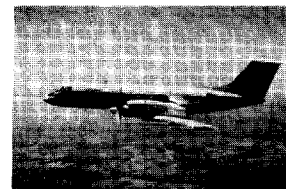
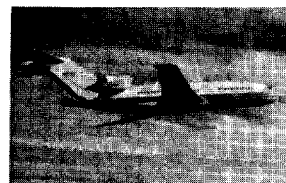


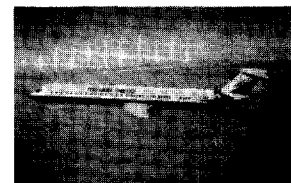
FIGURE 1. - NASA/INDUSTRY ADVANCED TURBOPROP (ATP) PROGRAM.



PTA/GULFSTREAM GII



UDF/BOEING 727



UDF/MD-80 AND  
578DX/MD-80

C-87-10471

FIGURE 2. - FLIGHT TESTING OF ADVANCED TURBOPROPS.

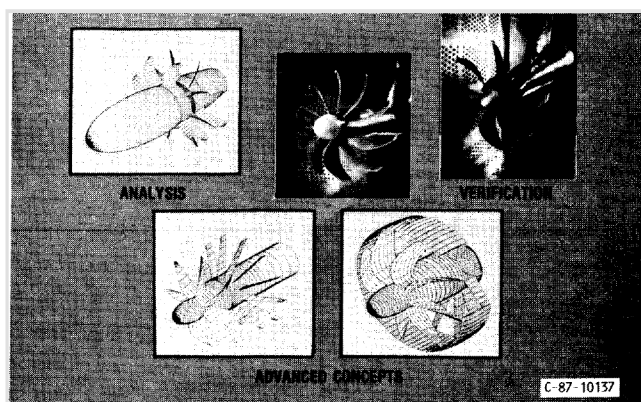


FIGURE 3. - POST-FLIGHT TEST AREAS OF ON-GOING PROPELLER RESEARCH AT NASA LEWIS RESEARCH CENTER.



FIGURE 4.- ADVANCED PROPELLER BLADE WIND TUNNEL MODELS.

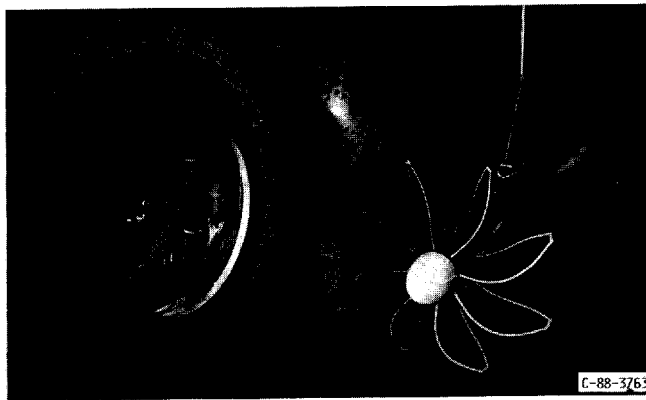


FIGURE 5. - SR-7A PROPELLER MODEL IN LEWIS 8- BY 6-FT. WIND TUNNEL.

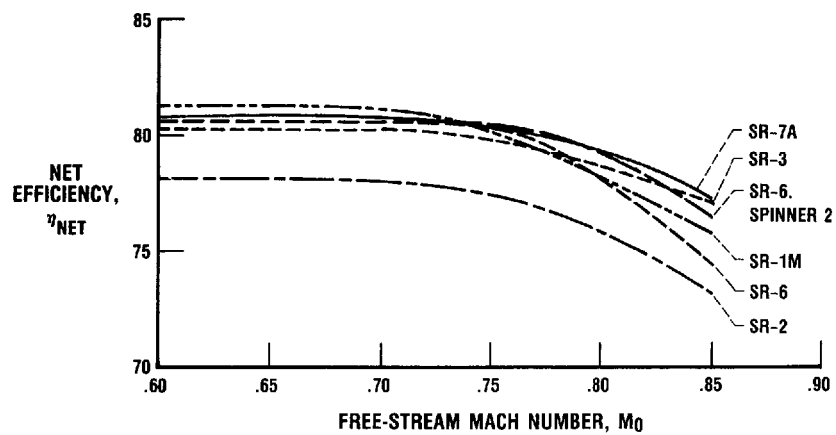


FIGURE 6. - SINGLE-ROTATION PROPELLER PERFORMANCE.

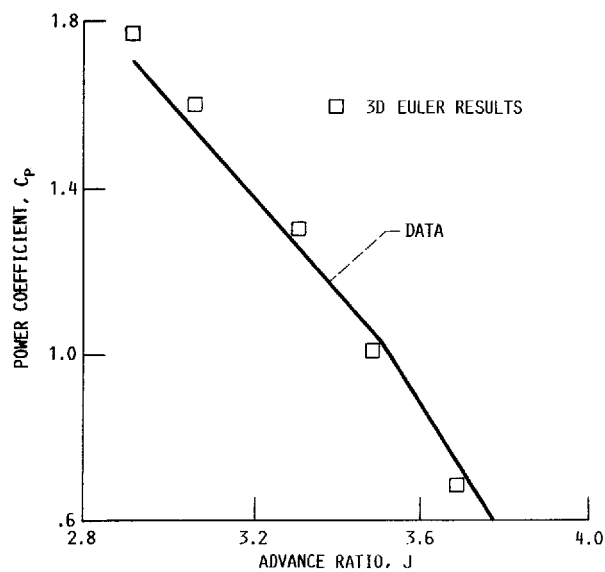


FIGURE 7. - POWER COEFFICIENT COMPARISON FOR SR-3 PROPELLER AT  $M = 0.8$ .

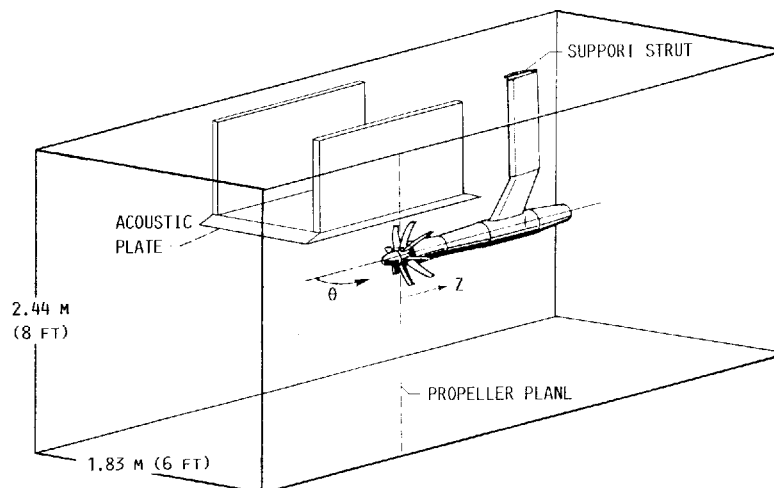
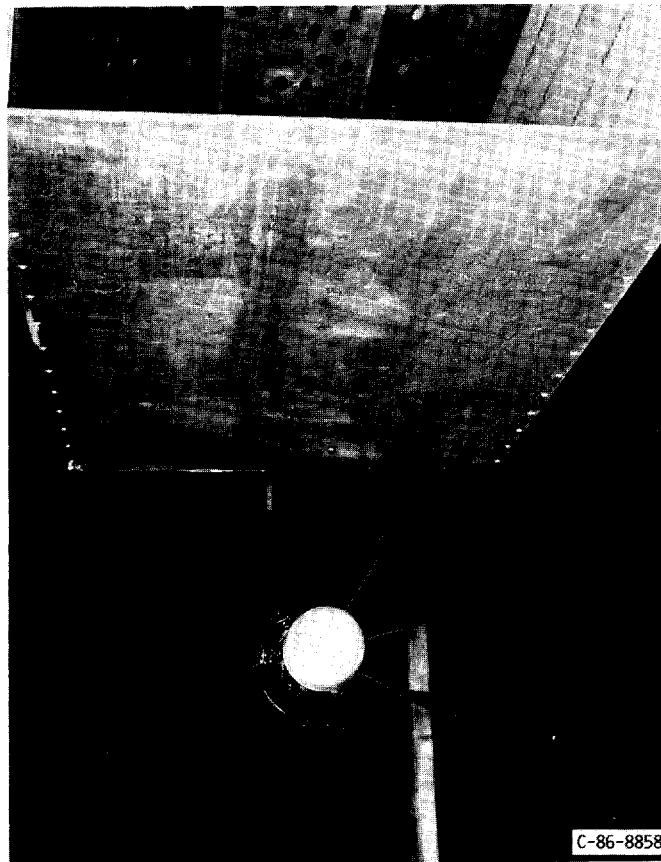


FIGURE 8. - ACOUSTIC PLATE IN NASA LEWIS 8- BY 6-FT. WIND TUNNEL.

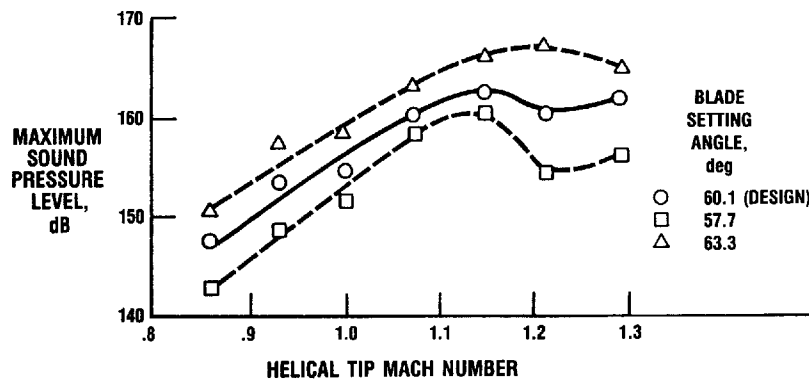


FIGURE 9. - SR-7 PEAK BLADE PASSING TONE VARIATION WITH HELICAL TIP MACH NUMBER; CONSTANT ADVANCE RATIO, 3.06.

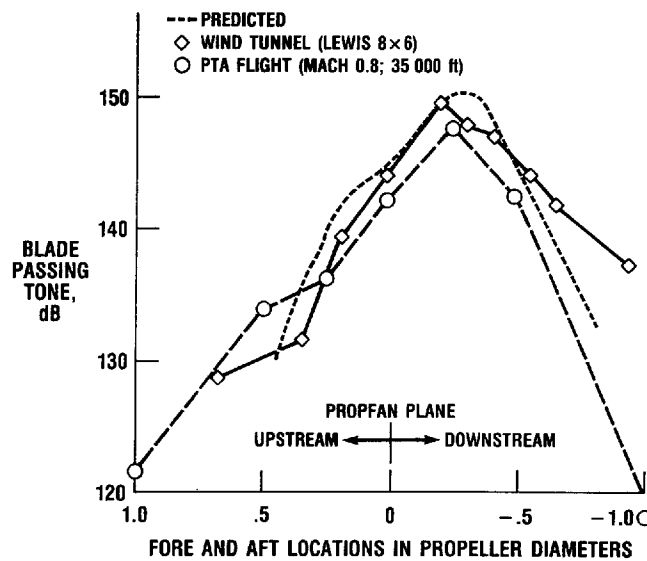


FIGURE 10. - COMPARISON OF PTA FUSELAGE SURFACE NOISE WITH PREDICTION AND WIND TUNNEL DATA.

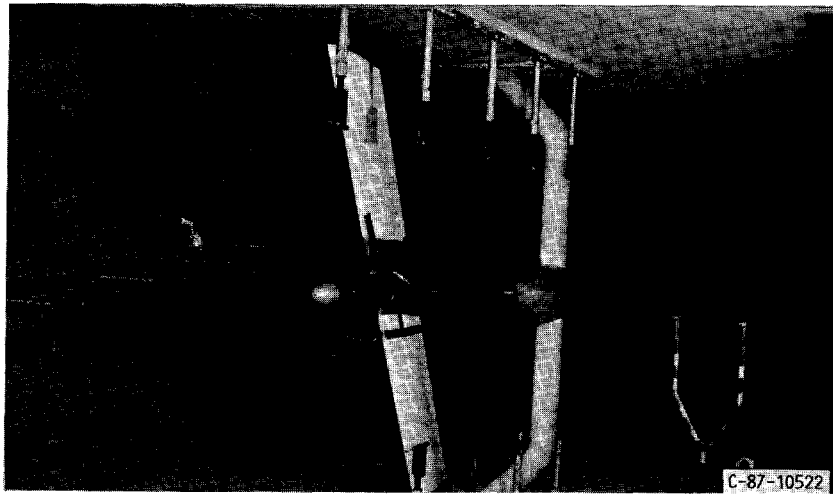


FIGURE 11. - SR-7A PROPELLER MODEL IN 9- BY 15-FT. ANECHOIC WIND TUNNEL.

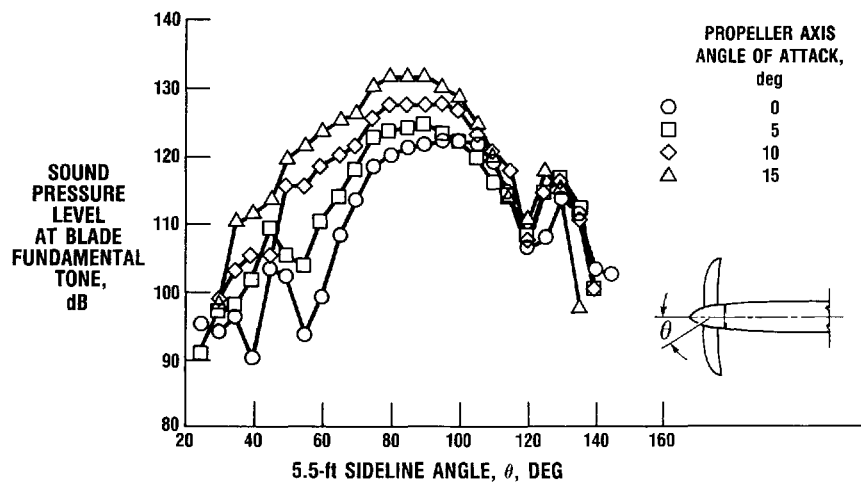


FIGURE 12. - EFFECT OF ANGLE OF ATTACK ON FLYOVER NOISE; SINGLE-ROTATION PROPELLER SR-7A; 9- BY 15-FT. WIND TUNNEL; TAKEOFF BLADE ANGLE,  $37.8^\circ$ ; TIP SPEED, 800 FT./SEC.; TUNNEL MACH NUMBER, 0.2.



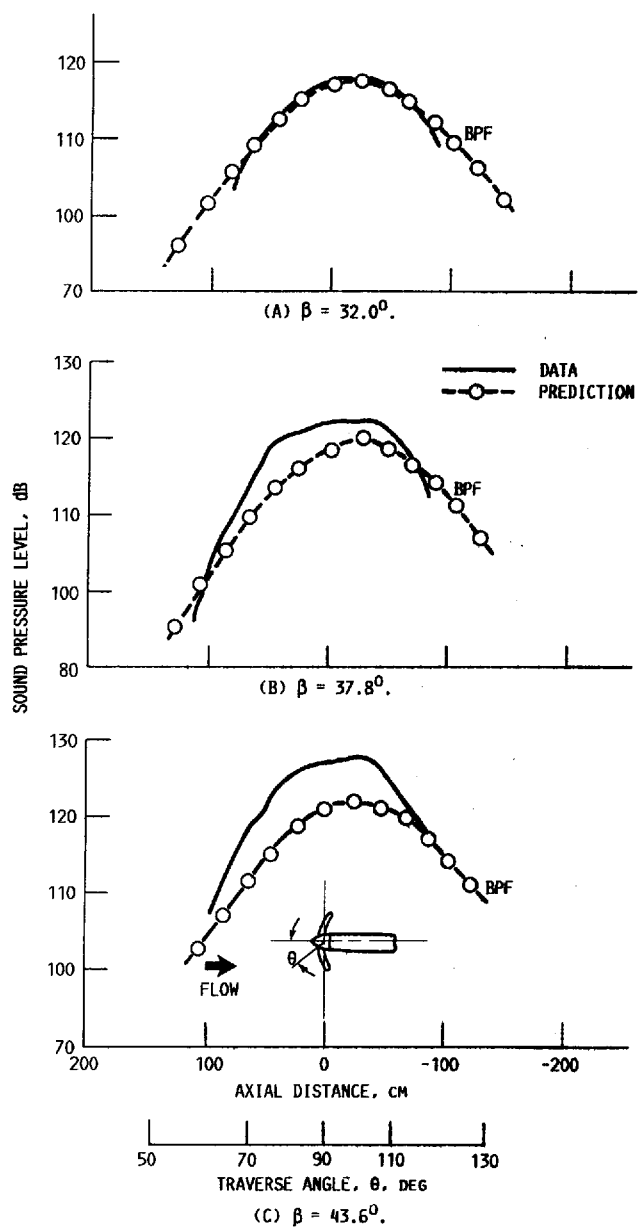


FIGURE 16. - COMPARISON OF SR-7A MODEL DATA WITH PREDICTION (1.68 M SIDELINE,  $J = 0.886$ ,  $M_0 = 0.2$ ).



FIGURE 17. - TWO-BLADE VERSION OF LARGE-SCALE ADVANCED PROPFAN (LAP).

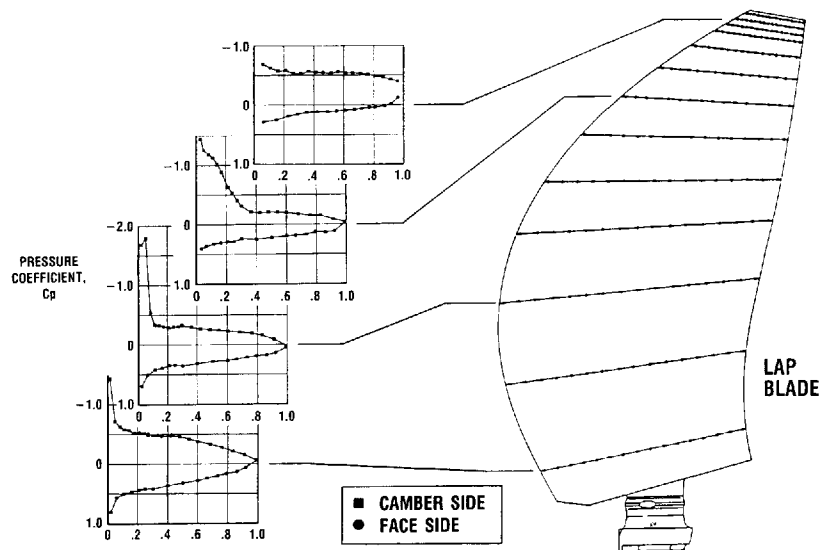


FIGURE 18. - BLADE PRESSURE MEASUREMENTS ON FULL SCALE PROPELLER; LOW-SPEED CONDITION



FIGURE 19. - VISUALIZATION OF PROPELLER BLADE SURFACE FLOW, OFF-DESIGN CONDITIONS.

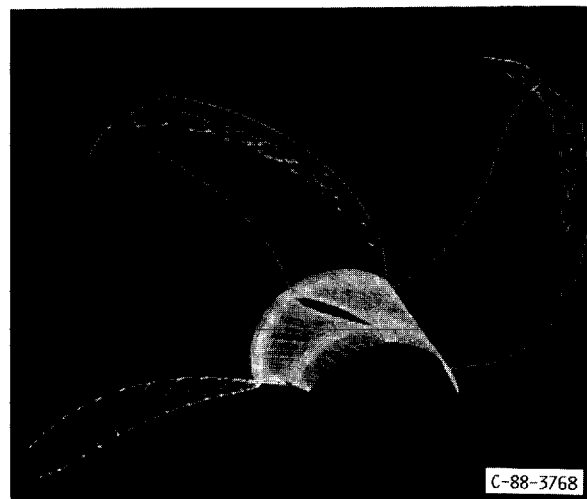


FIGURE 20. - COMPUTED STREAMLINES ON CRP-X1 PROPELLER, MACH 0.2;  $J = 1.0$ .

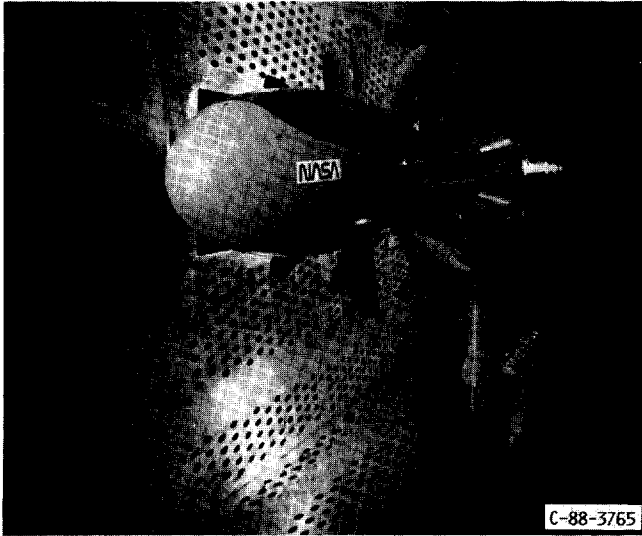


FIGURE 21. - UDF COUNTERROTATION PROPELLER MODEL IN NASA LEWIS 8- BY 6-FT. WIND TUNNEL.

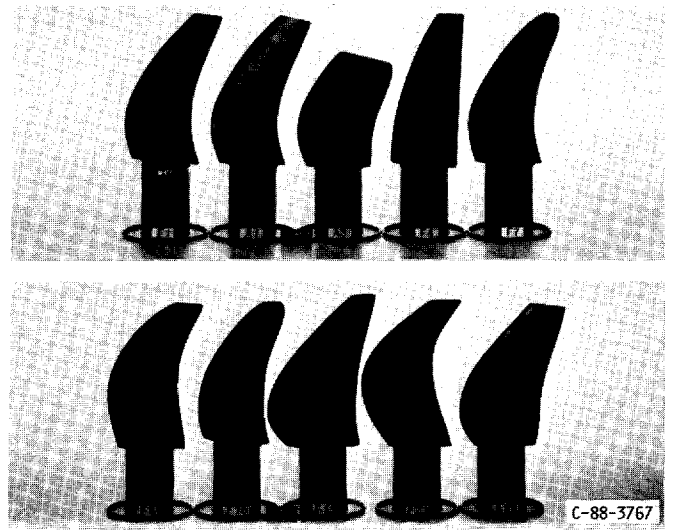


FIGURE 22. - WIND TUNNEL MODELS OF UDF COUNTERROTATION BLADE CONFIGURATIONS.

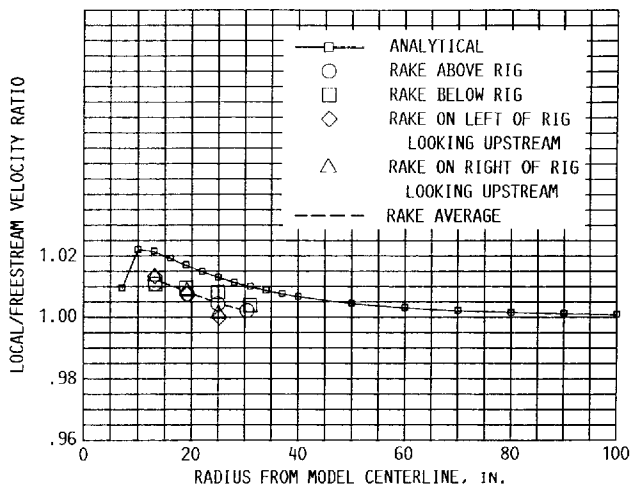


FIGURE 23. - COMPARISON OF ANALYTICAL AND EXPERIMENTAL VELOCITY RATIOS AROUND THE COUNTERROTATING PROPELLER TEST RIG AT THE PROPELLER PLANE AT MACH 0.80.

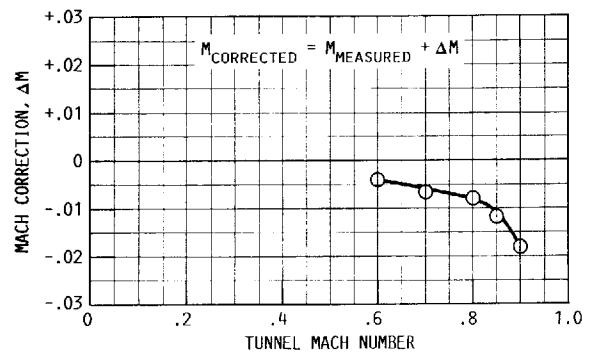


FIGURE 24. - MACH NUMBER INTERFERENCE CORRECTION FOR COUNTERROTATING PROPELLER TEST RIG IN POROUS WALL NASA LEWIS 8x6 FOOT WIND TUNNEL.

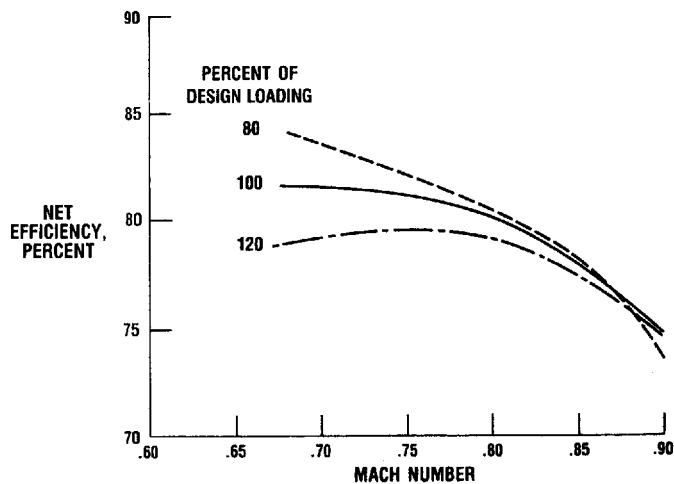


FIGURE 25. - F7/A7 PERFORMANCE SUMMARY; 8/8 BLADE CONFIGURATION; NOMINAL SPACING; MATCHED SPEED; 780 FT./SEC. TIP SPEED.

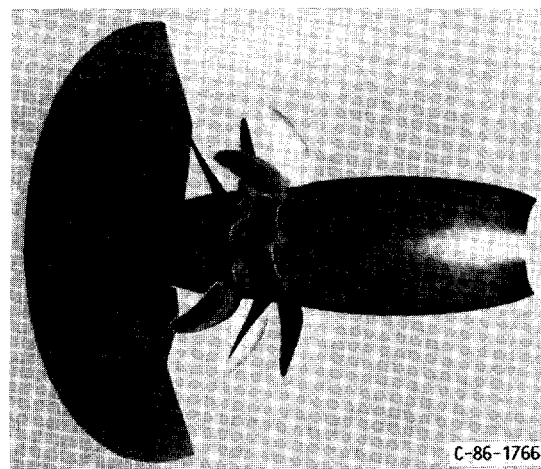


FIGURE 26. - THREE DIMENSIONAL EULER ANALYSIS OF COUNTER-ROTATIONAL PROPELLER FLOW FIELD.

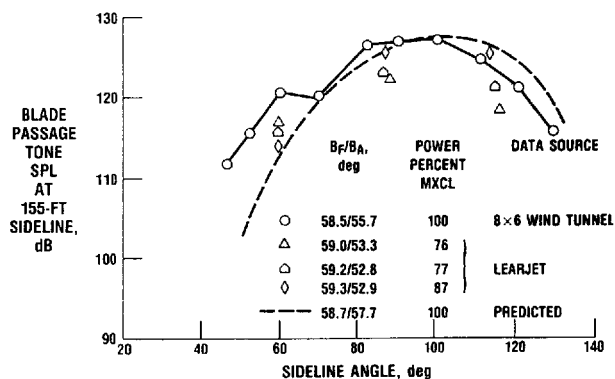


FIGURE 27. - UDF FUNDAMENTAL TONE DIRECTIVITY MEASURED IN FLIGHT, COMPARED WITH SCALED MODEL DATA AND PREDICTION; F7/A7 BLADE CONFIGURATION AT MACH 0.72 CRUISE CONDITIONS.

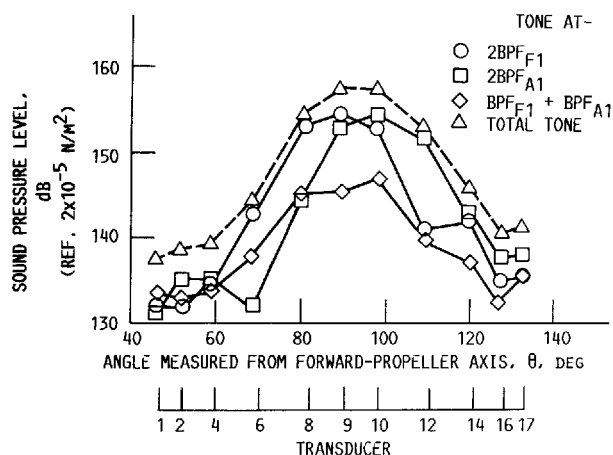


FIGURE 28. - SUMMATION OF TONES AT TWICE BLADE PASSING FREQUENCY; MACH 0.76 AND 100-PERCENT SPEED.  $F1/A1$ , 9/8.

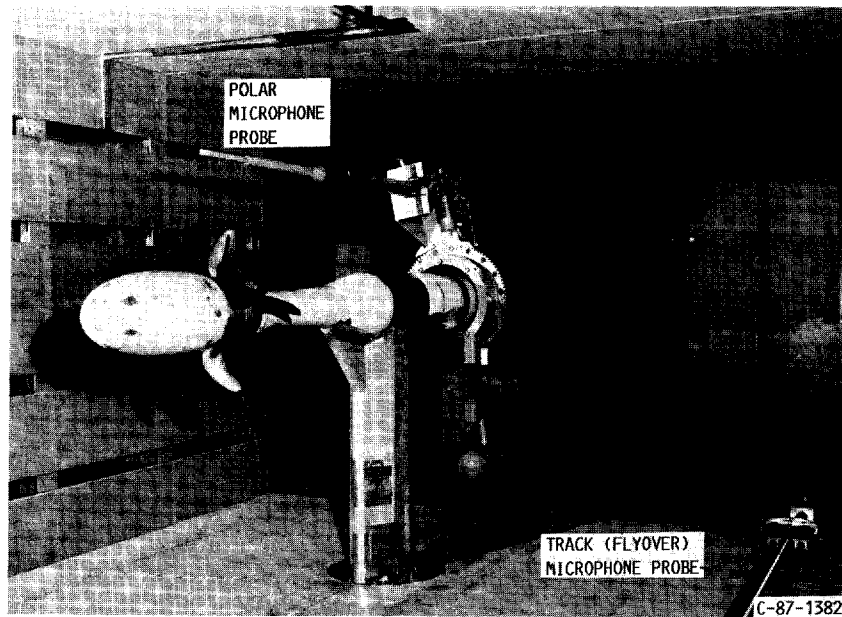


FIGURE 29. - PHOTOGRAPH OF THE UDF COUNTER-ROTATING TURBOPROP MODEL IN THE 9x15 ANECHOIC WIND TUNNEL.

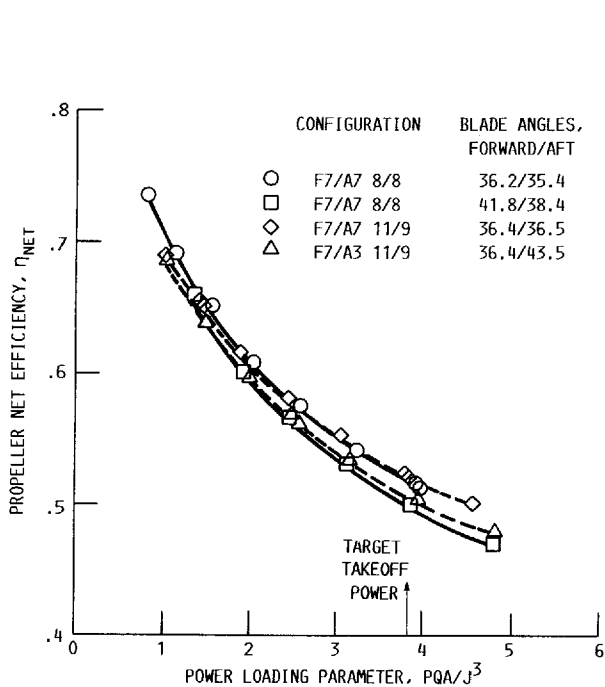


FIGURE 30. - COUNTERROTATION PROPELLER PERFORMANCE (TAKE-OFF TARGET OPERATING POINT POWER LOADING PARAMETER OF 3.830 AT MACH NUMBER 0.20).

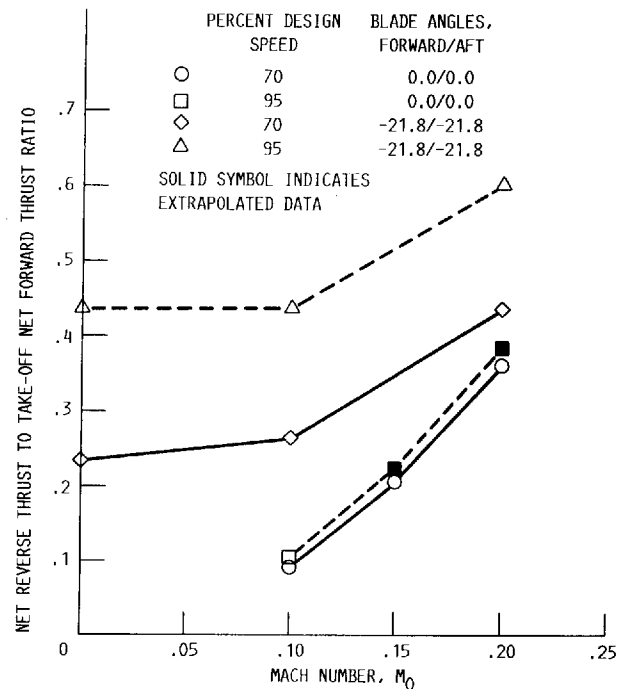


FIGURE 31. - EFFECT OF MACH NUMBER ON REVERSE THRUST PERFORMANCE OF F7/A7, 8/8 PROPELLER.

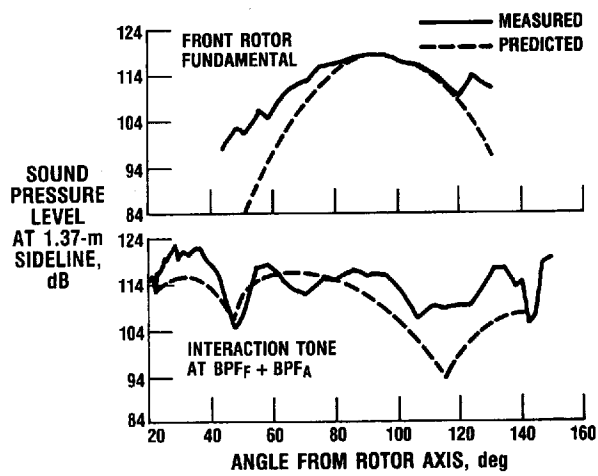


FIGURE 32. - COUNTERROTATION PROPELLER NOISE AT TAKEOFF; PROPELLER F7/A7; MACH 0.2; 9-BY 15-FT. WIND TUNEL.

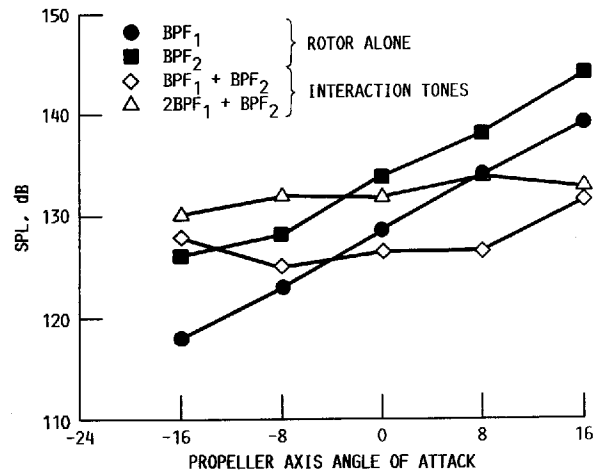


FIGURE 33. - ANGLE OF ATTACK EFFECTS ON COUNTERROTATION TONES IN AFT PROPELLER PLANE, BELOW THE AIRCRAFT. F7/A7, 11/9;  $B_1/B_2 = 36.4^0/36.5^0$ ; 90% SPD;  $M_\infty = 0.2$ .

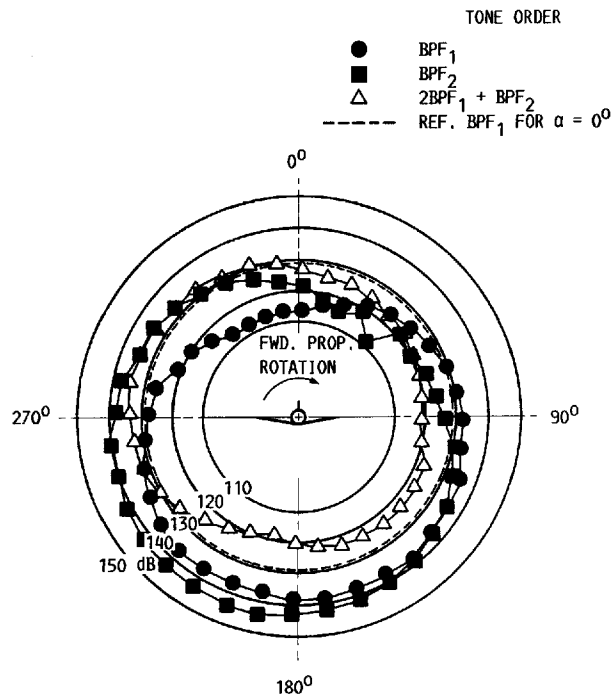


FIGURE 34. - CIRCUMFERENTIAL TONE DIRECTIVITY AT THE AFT PROPELLER PLANE FOR  $\alpha = 16^0$ . F7/A7, 11/9; 90 PERCENT SPD;  $B_1 = 36.4^0/36.5^0$ ; NOMINAL SPACING;  $M_\infty = 0.2$ .